# Paired charge-2 Weyl-Dirac phonons in tetragonal crystals

Peng Wu,[1] Guang Liu,[1] Xiangting Hu,[1] and Hu Xu[1,2,3,*]
[1]*Department of Physics, Southern University of Science and Technology, Shenzhen 518055, People's Republic of China*
[2]*Quantum Science Center of Guangdong-Hong Kong-Macao Greater Bay Area (Guangdong), Shenzhen 518045, People's Republic of China*
[3]*Shenzhen Key Laboratory for Advanced Quantum Functional Materials and Devices, Southern University of Science and Technology, Shenzhen 518055, People's Republic of China*

(Received 7 May 2023; revised 3 July 2023; accepted 1 August 2023; published 11 August 2023)

Unconventional Weyl and Dirac phonons with topological charges of ±2 have attracted significant attention due to their exceptional properties. By employing a minimal lattice model, we propose that an ideal topological quasiparticle coexistence system can be achieved in chiral space groups 92 and 96. This system specifically incorporates a charge-2 Weyl phonon and a charge-2 Dirac phonon. Notably, the crystal symmetry restricts these two topological quasiparticles to high-symmetry points within the Brillouin zone, resulting in an ultralong surface arc that extends across the entire surface Brillouin zone. Moreover, the topological surface arcs exhibit a unique saddlelike surface feature. Taking $BaPt_2S_3$ as a representative example, we validate our prediction and reveal the interconnected ultralong surface arc and saddlelike topological surface state. Our work establishes a valuable framework for investigating diverse types of double Weyl nodes and presents a promising approach for detecting ultralong surface arcs.

DOI: 10.1103/PhysRevB.108.054305

## I. INTRODUCTION

In recent decades, the classification of materials based on topology and symmetry has rapidly advanced into gapless systems, giving rise to distinct topological phases [1–3], such as zero-dimensional Weyl points (WPs) [4–7] and Dirac points (DPs) [8–12], one-dimensional (1D) nodal lines [13–17], and two-dimensional (2D) nodal surfaces [18–20]. WP and DP quasiparticles have attracted widespread attention due to their similarities with high-energy physics counterparts. WPs are characterized by isolated nodal points of two nondegenerate bands, acting as magnetic monopoles in momentum space and carrying a quantized topological charge (i.e., Chern number $C$) of ±1. These unique topological features lead to various fascinating transport properties, including negative magnetoresistive effects [21–23] and anomalous Hall effects [24–27]. Specifically, WPs cannot be annihilated but can be paired with opposite topological charges at the same momentum position, forming a DP.

The discovery of novel quasiparticles in condensed matter [28] exhibiting a chirality greater than 1 and lacking a direct counterpart in high-energy physics has sparked intense study. Among these, double Weyl nodes [29–34] with a topological charge of ±2 are of particular interest and can be classified into three types. The first type, charge-2 WPs (CWPs) [see Fig. 1(a)], are twofold degenerate points carrying a Chern number $C$ of ±2. The second type, the spin-1 WPs [see Fig. 1(b)], consist of a linear Weyl cone crossed with an additional flat band, carrying $C$ values of +2, 0, and −2, respectively. The third type, charge-2 Dirac points (CDPs) [see Fig. 1(c)], are fourfold band crossings with linear dispersion in any direction, carrying $C = \pm 2$.

Phonons, being bosons, do not adhere to the Pauli exclusion principle, making topological phonons observable across the entire frequency range in solids. This has led to the discovery of various topological phonon states, such as type-II Weyl phonons [35], charge-4 Weyl phonons [36], helical nodal line phonons [37], type-III nodal ring phonons [38], topological gimbal phonons [39], and phononic obstructed atomic insulators [40]. Recent studies have reported systems with multiple particles [41–51], confirming that different types of topological phonon states can coexist within a single system. However, studies involving the coexistence of CWPs and CDPs in a single system are lacking. Moreover, a high number of Weyl nodes within a system can result in indistinguishable surface arcs, making experimental observations challenging. Consequently, concise and paired systems with clear surface arcs are gaining popularity.

In this work, we construct a minimal lattice model and confirm the existence of single-pair systems featuring a CWP and a CDP in chiral space groups 92 and 96. By analyzing the effective Hamiltonian, we confirm that both CWPs and CDPs are necessarily degenerate due to symmetry protection. Examining the projected phonon surface states, we observe an ultralong surface arc connecting the CWP and CDP, spanning the entire surface Brillouin zone (BZ). Using first-principles calculations, we propose nine materials as promising candidates for studying single-pair systems of CWPs and CDPs, featuring ultralong surface arcs. Our work provides an intriguing platform for further study of double Weyl phonon nodes.

*xuh@sustech.edu.cn

 

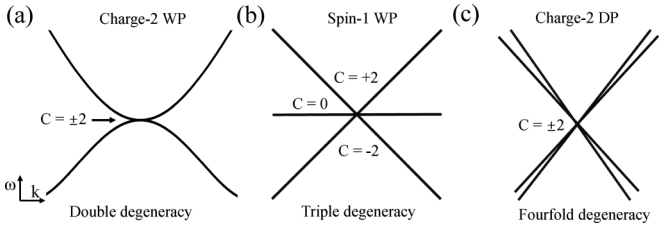


FIG. 1. Three types of double Weyl nodes: (a) charge-2 WP, (b) spin-1 WP, and (c) charge-2 DP.

## II. RESULTS AND DISCUSSION

To better understand the performance of single-pair systems, the minimal lattice model (tight binding) is preferred [52–55]. Based on the relationship between Wyckoff position and band representation, we explicitly construct a four-band lattice model for $P4_12_12$ (No. 92), as shown in Fig. 2(a). The symmetry generators include $\widetilde{C}_{4z} \equiv \{C_{4z}|\frac{1}{2}\frac{1}{2}\frac{1}{4}\}$, $\widetilde{C}_{2y} \equiv \{C_{2y}|\frac{1}{2}\frac{1}{2}\frac{1}{4}\}$, and time inversion symmetry $\mathcal{T}$. The unit cell contains four sites located at the $4a$ Wyckoff position, indicated by blue balls labeled as $A_i$ (where $i = 1, 2, 3, 4$) and the four sites at positions $\{(\frac{1}{2}, \frac{1}{2}, \frac{3}{4}), (0, 0, 0), (0, 0, \frac{1}{2}), (\frac{1}{2}, \frac{1}{2}, \frac{1}{4})\}$. With this basis set, the lattice operator can be represented as follows:

$$D(\widetilde{C}_{4z}) = \begin{pmatrix} 0 & 0 & 1 & 0 \\ 1 & 0 & 0 & 0 \\ 0 & 0 & 0 & 1 \\ 0 & 1 & 0 & 0 \end{pmatrix}, \quad D(\widetilde{C}_{2y}) = \sigma_1 \otimes \tau_0,$$
$$D(\mathcal{T}) = \mathcal{K}, \tag{1}$$

where $\sigma_i$, $\tau_j$ are Pauli matrices, and $\mathcal{K}$ is the complex conjugate operator. Then, the $4 \times 4$ lattice Hamiltonian can be constructed using the above symmetries [56]:

$$\begin{aligned} H =& (t_1 - t_2)\Big[\sin\frac{k_z}{4}\Big(\cos\frac{k_x}{2}\sin\frac{k_y}{2}\Gamma_{31} + \sin\frac{k_x}{2}\cos\frac{k_y}{2}\Gamma_{13}\Big) \\ &+ \cos\frac{k_z}{4}\Big(\cos\frac{k_x}{2}\sin\frac{k_y}{2}\Gamma_{02} - \sin\frac{k_x}{2}\cos\frac{k_y}{2}\Gamma_{20}\Big)\Big] \\ &+ (t_1 + t_2)\Big[\cos\frac{k_x}{2}\cos\frac{k_y}{2}\cos\frac{k_z}{4}(\Gamma_{01} + \Gamma_{10}) \\ &- \cos\frac{k_x}{2}\cos\frac{k_y}{2}\sin\frac{k_z}{4}(\Gamma_{32} - \Gamma_{23})\Big] + t_3\cos\frac{k_z}{2}\Gamma_{11} \\ &+ [t_4 + t_5(\cos k_x + \cos k_y)]\Gamma_{00}, \end{aligned} \tag{2}$$

where $t_{1,2,3,4,5}$ are real parameters and $\Gamma_{i,j} = \sigma_i \otimes \tau_j$. It can be verified that the Hamiltonian (2) remains invariant under the above operations.

We calculate the phonon dispersion for this lattice model and plot them in Fig. 2(c). The corresponding bulk BZ is shown in Fig. 2(b), where the green and orange squares depict the BZ projections in the (001) and (010) directions, respectively. Here, we focus on the Γ point and $A$ point with highlighted squares. Clearly, the two middle bands degenerate at the Γ point, featuring quadratic dispersion in the $k_x$-$k_y$ plane and linear dispersion in the $k_z$ direction. Two doubly degenerate states along the high-symmetry line converge to form a fourfold degenerate point at the $A$ point, displaying

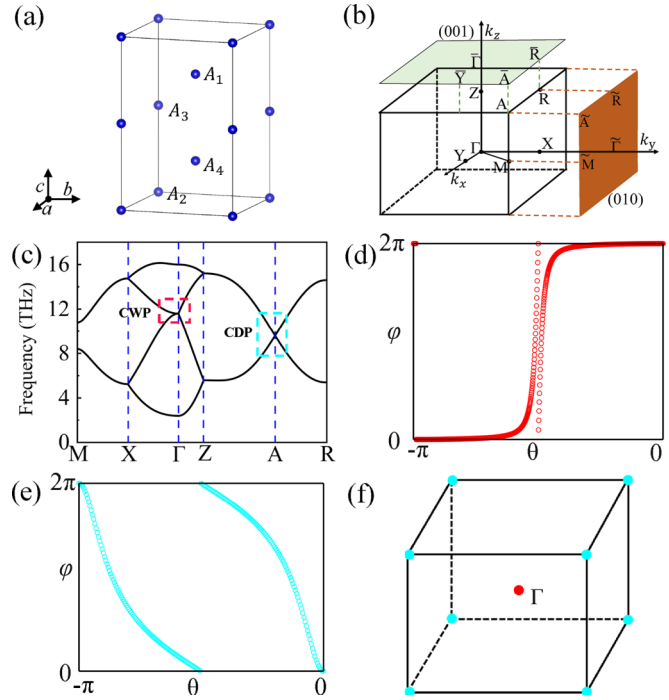


FIG. 2. Four-band lattice model for space group 92: (a) perspective view of the primitive unit cell, (b) bulk BZ and surface BZs, (c) calculated band structure, (d) evolution of Wannier charge centers (WCCs) for the CWP, (e) WCCs for the CDP, and (f) degradation modes between the two middle phonon spectra with red and cyan dots representing CWP and CDP, respectively. In the calculation, $t_1 = 4, t_2 = -0.6, t_3 = -1.2, t_4 = 10, t_5 = 0.2$.

linear dispersion. To confirm the topological charge of these topologically protected nodes, the Wilson loop approach [57] is performed to calculate the Chern numbers of nodes. As shown in Figs. 2(d) and 2(e), we can verify that the double degenerate point at Γ contributes a Chern number $C = +2$ and the Chern number of the four-band degenerate point at $A$ is $C = -2$, which confirms a CWP at the Γ point and a CDP at the $A$ point.

We further examine the degenerate nodes of the middle two bands, as shown in Fig. 2(f). Each CDP at the $A$ point contributes 1/8 of the topological charge, and the total topological charge of the CDP is $-2$, in contrast to the CWP at the Γ point with a topological charge of $+2$. The total topological charge is zero, in accordance with the "no-go" theorem. Furthermore, the system has only one pair of degenerate points belonging to different double Weyl types with opposite topological charges. Such a simple yet feature-rich system fits perfectly into the mindset of physics with "minimum numbers," inspiring further exploration. The degenerate properties of the phonon band at the Γ and $A$ points are extremely stable and exhibit necessary degeneracy. Thus, we can randomly select parameters within a reasonable range and ensure that the degenerate case appears as a natural result. To identify topologically protected phonon states, we construct the low-energy effective Hamiltonian model for the Γ point and $A$ point. The little group at the Γ point is $D_4$, which has an intrinsic two-dimensional irreducible representation (IR) $R_5$ [58], thus enforcing a doubly degenerate band point. At

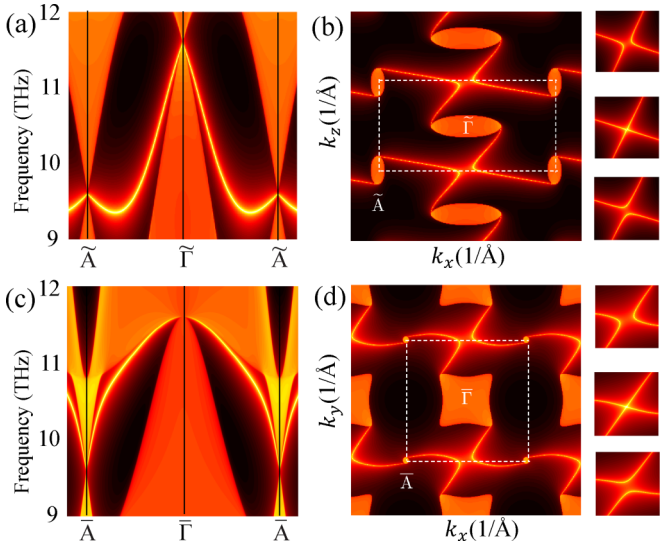


FIG. 3. Topological phonon surface states of the lattice model: phonon LDOS projected on the (a) (010) and (c) (001) surfaces; isofrequency surface arcs projected on the (b) (010) and (d) (001) surfaces. In (b) [(d)], the isofrequency surface arcs are plotted at the frequency of 10.18 (9.98) THz, and the right panels are plotted at the frequencies of 10.18 (9.98), 10.195 (10.00), and 10.21 (10.02) THz, from top to bottom, respectively.

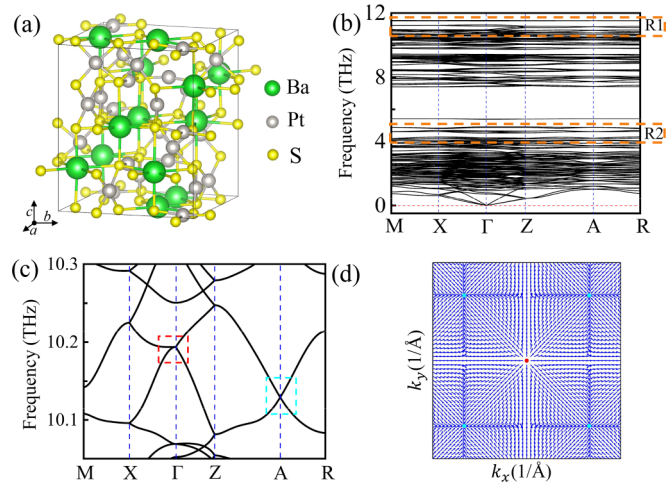


FIG. 4. (a) Crystalline structure of $BaPt_2S_3$. (b) Phonon spectra along high-symmetry lines and (c) schematic illustration of phonon dispersion in the R1 region. (d) Distribution of Berry curvature in the $k_x$-$k_y$ plane with red and cyan points denoting CWP and CDP, respectively.

the $A$ point, there is a pair of two-dimensional conjugate IRs that can be connected to each other under $\mathcal{T}$, forming a four-dimensional IR and resulting in a fourfold degenerate point (see more details in the Supplemental Material (SM) [59]).

The topological phonon nodal points with nonzero Chern numbers lead to unique nontrivial surface arcs. We employ the iterative Green's function method to calculate phonon surface states. Unlike the conventional pair of WPs with opposite topological charges exhibiting internally linked performance, the phonon local density of states (LDOS) projected on the (010) surface shows that the surface arc connects the projection point $\bar{\Gamma}$ of the CWP and the projection point $\bar{A}$ of the CDP, further extending continuously across adjacent BZs [see Fig. 3(a)]. Due to the requirement of topological charge conservation, the surface arc at the boundary of the originating CDP at the $A$ point shares the CWP of neighboring Wigner-Seitz cells, further confirmed by the isofrequency surface of (010) shown in Fig. 3(b). The surface arc resembles an ultralong chain that spans the entire surface BZ without terminal. Notably, the surface states exhibit a saddlelike characteristic, highlighted by the enlarged surface arc panels on the right-hand side of (b). From the bottom to the top, with a gradual increase in frequency, the surface arcs of the two branches intersect and then separate along another direction, a typical feature of saddlelike contours. Additionally, the (010) projected surface reveals that both CWP and CDP are linearly dispersive along the $k_z$ direction. We also plot the LDOS and isofrequency surface projected on the (001) surface in Figs. 3(c) and 3(d), respectively. Similar to the (010) case, the ultralong surface arc connects the CWP (projected to $\bar{\Gamma}$) and CDP (projected to $\bar{A}$) and also displays the saddlelike characteristic. The single pairs of CWP and CDP discussed above are fascinating, and more cases are anticipated. The lattice model for space group (SG) 96 exhibits the coexistence features of CWP and CDP, akin to the topological behavior for SG 92, which can be viewed in the SM [59]. Also, two phonon branches with different eigenvalues that satisfy certain relations intersect along the $\widetilde{C}_{4z}$ invariant path $\Gamma - A$, supporting a CWP. This is an accidental case and not easily demonstrated directly by the lattice model. Therefore, we discuss it using the $\boldsymbol{k} \cdot \boldsymbol{p}$ method in the SM [59].

Based on the above theoretical analysis, we confirm that a series of materials satisfy the single-pair system using first-principles calculations. Here, we mainly focus on $BaPt_2S_3$, with other candidates provided in the SM [59]. As shown in Fig. 4(a), the crystal structure belongs to the chiral space group $P4_22_12$ (No. 92), and each unit cell contains 12 Ba, 24 Pt, and 36 S atoms. The optimized lattice constants are $a = 11.19$ Å and $c = 13.31$ Å. $BaPt_2S_3$ has already been synthesized from a flow of sulfur-containing argon from $BaPt(CN)_4$-$2H_2O$ [60]. The corresponding BZ is the same as in Fig. 2(b).

As shown in Fig. 4(b), we plot the phonon spectrum for $BaPt_2S_3$. There are no imaginary vibrational modes in the BZ, confirming its dynamical stability. Interestingly, the material contains two frequency ranges that correspond to the single-pair system, identified as the R1 and R2 regions. Here, we observe a single-pair system in the R1 region with frequencies of 10.10–10.20 THz, and the features of the R2 region are demonstrated in the SM [59]. In Fig. 4(c), we present an enlarged view of the phonon spectrum within the R1 region. At the $A$ point, a crossing point with linear dispersion is formed by four phonon branches, covering modes ranging from the 177th to the 180th. The two middle branches cross at the $\Gamma$ point, exhibiting linear dispersion along the $k_z$ direction and quadratic dispersion in the $k_x$-$k_y$ plane. The crossing frequencies at the $\Gamma$ and $A$ points are $\omega_\Gamma = 10.14$ and $\omega_A = 10.19$ THz, respectively. We have examined the degeneracy of the phonon spectrum across the entire BZ and verified the absence of any additional quasiparticles. Furthermore, the

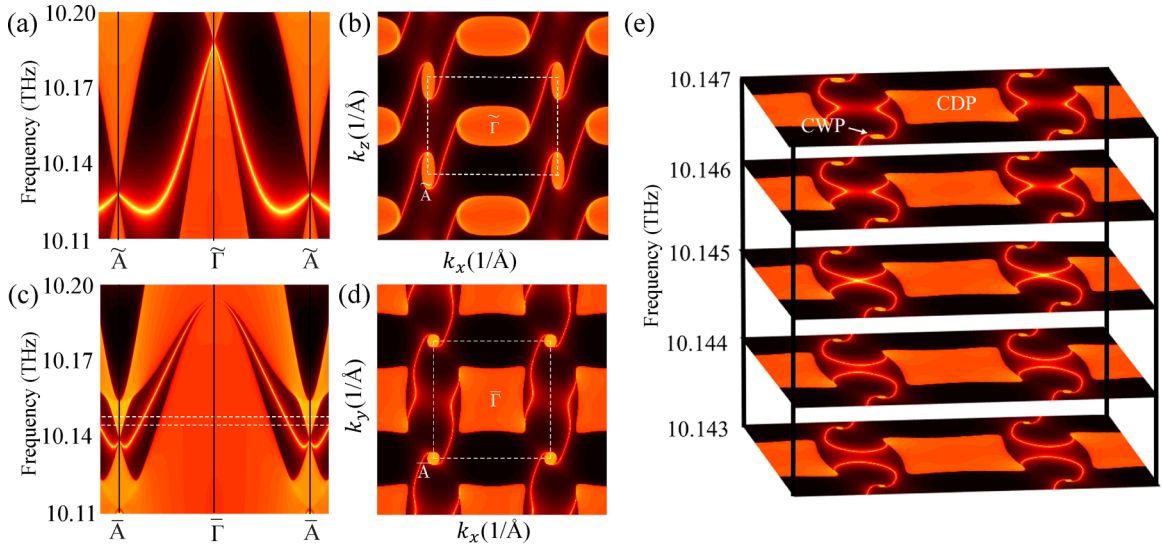


FIG. 5. Phonon LDOS projected on the (a) (010) and (c) (001) surfaces. Isofrequency surface arcs at 10.15 THz projected on the (b) (010) and (d) (001) surfaces. In (c), the white line indicates the selected frequency range for observing the evolution of the saddlelike surface states with increasing frequency, as shown in (e).

significant separation between the CWP and CDP at both the center and boundary of the BZ provides an excellent opportunity for further observations. Chiral charge calculations reveal that the twofold degeneracy at the Γ point possesses a topological charge of +2, corresponding to CWP, and the fourfold degeneracy at the $A$ point has a topological charge of −2, corresponding to CDP. In Fig. 4(d), the distribution of Berry curvature in the $k_x$-$k_y$ plane is plotted, revealing that the CWP at the Γ point can be considered as the "source" point, while the CDP at the $A$ point acts as the "sink" point in momentum space, respectively.

As shown in Fig. 5(a), a visible surface arc on the LDOS projected (010) surface links the projection points $\widetilde{\Gamma}$ and $\widetilde{A}$. Further evidence of this ultralong link performance is provided by the isofrequency contour of the (010) surface at 10.15 THz in Fig. 5(b). The alternating connections between the origin and end projection points cause the surface arc to span the entire momentum space. Similarly, ultralong surface arc features can be observed on the (001) projection surface of the LDOS in Fig. 5(c) and isofrequency contour in Fig. 5(d), respectively. In Fig. 5(e), we observe the evolution of saddlelike surface states with increasing frequency by choosing five contours projected onto the (001) surface. The two branch surface arcs gradually intersect and then separate, with the critical isofrequency surface corresponding to the occurrence of the Lifshitz-like transition at $\omega = 10.145$ THz, confirming the saddlelike feature. As expected, all topological properties discussed above for $BaPt_2S_3$ in the R1 region are consistent with our lattice model. Additional topological properties of the material are shown in the SM [59]. Furthermore, the ultralong phonon surface arc traversing the entire BZ provides a robust nontrivial one-way phonon propagation channel, which holds great promise for experimental implementation and further applications.

## III. CONCLUSIONS

In summary, we propose a single-pair system consisting of a charge-2 Weyl phonon and a charge-2 Dirac phonon in chiral space. Using minimal lattice model calculations, we determine that the charge-2 Weyl phonon and charge-2 Dirac phonon occupy separate high-symmetry points Γ and $A$, respectively. To explain the formation mechanism, we construct effective Hamiltonian models for each point. Moreover, our results reveal an ultralong surface arc spanning the entire surface Brillouin zone, exhibiting a distinctive saddlelike feature. Utilizing first-principles calculations, we identify nine materials with ultralong and clear surface states as candidates, confirming the widespread availability of single-pair systems in solid materials. Our work sheds light on the interplay between charge-2 Weyl phonons and charge-2 Dirac phonons, providing a platform for investigating the coexistence of various types of double Weyl phonon systems.

## ACKNOWLEDGMENTS

This work is supported by the National Key R&D Program of China (Grant No. 2022YFA1403700), the National Natural Science Foundation of China (Grant No. 11974160), the Science, Technology, and Innovation Commission of Shenzhen Municipality (Grant No. RCYX20200714114523069), and the Center for Computational Science and Engineering at Southern University of Science and Technology.

[1] Z.-M. Yu, Z. Y. Zhang, G. B. Liu, W. K. Wu, X. P. Li, R. W. Zhang, S. A. Yang, and Y. G. Yao, Sci. Bull. **67**, 375 (2022).

[2] Y. F. Xu, M. G. Vergniory, D. S. Ma, J. L. Mañes, Z. D. Song, B. A. Bernevig, N. Regnault, and L. Elcoro, arXiv:2211.11776.

[3] T. Yang, Y. Yang, X. T. Wang, G. Zhang, and Z. Cheng, Mater. Today Chem. **30**, 101488 (2023).

[4] X. G. Wan, A. M. Turner, A. Vishwanath, and S. Y. Savrasov, Phys. Rev. B **83**, 205101 (2011).

[5] H. M. Weng, C. Fang, Z. Fang, B. A. Bernevig, and X. Dai, Phys. Rev. X **5**, 011029 (2015).

[6] S. Y. Xu, I. Belopolski, N. Alidoust, M. Neupane, G. Bian, C. L. Zhang, R. Sankar, G. Q. Chang, Z. Yuan, C. C. Lee *et al.*, Science **349**, 613 (2015).

[7] B. Q. Lv, S. Muff, T. Qian, Z. D. Song, S. M. Nie, N. Xu, P. Richard, C. E. Matt, N. C. Plumb, L. X. Zhao *et al.*, Phys. Rev. Lett. **115**, 217601 (2015).

[8] Z. J. Wang, Y. Sun, X. Q. Chen, C. Franchini, G. Xu, H. M. Weng, X. Dai, and Z. Fang, Phys. Rev. B **85**, 195320 (2012).

[9] Z. J. Chen, R. Wang, B. W. Xia, B. B. Zheng, Y. J. Jin, Y. J. Zhao, and H. Xu, Phys. Rev. Lett. **126**, 185301 (2021).

[10] W. J. Wu, Y. Xie, and Y. P. Chen, Phys. Rev. Mater. **5**, 104201 (2021).

[11] H. L. He, C. Qiu, L. P. Ye, X. X. Cai, X. Fan, M. Z. Ke, F. Zhang, and Z. Y. Liu, Nature (London) **560**, 61 (2018).

[12] S. M. Young, S. Zaheer, J. C. Y. Teo, C. L. Kane, E. J. Mele, and A. M. Rappe, Phys. Rev. Lett. **108**, 140405 (2012).

[13] R. Yu, H. M. Weng, Z. Fang, X. Dai, and X. Hu, Phys. Rev. Lett. **115**, 036807 (2015).

[14] Y. Kim, B. J. Wieder, C. L. Kane, and A. M. Rappe, Phys. Rev. Lett. **115**, 036806 (2015).

[15] H. M. Weng, Y. Y. Liang, Q. N. Xu, R. Yu, Z. Fang, X. Dai, and Y. Kawazoe, Phys. Rev. B **92**, 045108 (2015).

[16] G. Liu, Y. J. Jin, Z. J. Chen, and H. Xu, Phys. Rev. B **104**, 024304 (2021).

[17] X. T. Wang, T. Yang, Z. X. Cheng, G. Surucu, J. H. Wang, F. Zhou, Z. Y. Zhang, and G. Zhang, Appl. Phys. Rev. **9**, 041304 (2022).

[18] W. K. Wu, Y. Liu, S. Li, C. Y. Zhong, Z. M. Yu, X. L. Sheng, Y. X. Zhao, and S. A. Yang, Phys. Rev. B **97**, 115125 (2018).

[19] Q. F. Liang, J. Zhou, R. Yu, Z. Wang, and H. M. Weng, Phys. Rev. B **93**, 085427 (2016).

[20] X. M. Zhang, Z. M. Yu, Z. M. Zhu, W. K. Wu, S. S. Wang, X. L. Sheng, and S. A. Yang, Phys. Rev. B **97**, 235150 (2018).

[21] D. T. Son and B. Z. Spivak, Phys. Rev. B **88**, 104412 (2013).

[22] N. P. Armitage, E. J. Mele, and A. Vishwanath, Rev. Mod. Phys. **90**, 015001 (2018).

[23] J. Cano, B. Bradlyn, Z. Wang, M. Hirschberger, N. P. Ong, and B. A. Bernevig, Phys. Rev. B **95**, 161306(R) (2017).

[24] Q. Wang, Y. F. Xu, R. Lou, Z. H. Liu, M. Li, Y. B. Huang, D. W. Shen, H. M. Weng, S. C. Wang, and H. C. Lei, Nat. Commun. **9**, 3681 (2018).

[25] E. K. Liu, Y. Sun, N. Kumar, L. Muechler, A. Sun, L. Jiao, S. Y. Yang, D. F. Liu, A. J. Liang, Q. N. Xu *et al.*, Nat. Phys. **14**, 1125 (2018).

[26] W. Shi, L. Muechler, K. Manna, Y. Zhang, K. Koepernik, R. Car, J. van den Brink, C. Felser, and Y. Sun, Phys. Rev. B **97**, 060406(R) (2018).

[27] P. G. Li, J. Koo, W. Ning, J. G. Li, L. X. Miao, L. J. Min, Y. L. Zhu, Y. Wang, N. Alem, C. X. Liu *et al.*, Nat. Commun. **11**, 3476 (2020).

[28] B. Bradlyn, J. Cano, Z. J. Wang, M. G. Vergniory, C. Felser, R. J. Cava, and B. A. Bernevig, Science **353**, aaf5037 (2016).

[29] D. Takane, Z. Wang, S. Souma, K. Nakayama, T. Nakamura, H. Oinuma, Y. Nakata, H. Iwasawa, C. Cacho, T. Kim *et al.*, Phys. Rev. Lett. **122**, 076402 (2019).

[30] H. Miao, T. T. Zhang, L. Wang, D. Meyers, A. H. Said, Y. L. Wang, Y. G. Shi, H. M. Weng, Z. Fang, and M. P. M. Dean, Phys. Rev. Lett. **121**, 035302 (2018).

[31] C. Fang, M. J. Gilbert, X. Dai, and B. A. Bernevig, Phys. Rev. Lett. **108**, 266802 (2012).

[32] Z. C. Rao, H. Li, T. T. Zhang, S. J. Tian, C. H. Li, B. B. Fu, C. Y. Tang, L. Wang, Z. L. Li, W. H. Fan *et al.*, Nature (London) **567**, 496 (2019).

[33] D. S. Sanchez, I. Belopolski, T. A. Cochran, X. Xu, J.-X. Yin, G. Q. Chang, W. W. Xie, K. Manna, V. Süß, C-Y. Huang *et al.*, Nature (London) **567**, 500 (2019).

[34] T. T. Zhang, Z. D. Song, A. Alexandradinata, H. M. Weng, C. Fang, L. Lu, and Z. Fang, Phys. Rev. Lett. **120**, 016401 (2018).

[35] B. W. Xia, R. Wang, Z. J. Chen, Y. J. Zhao, and H. Xu, Phys. Rev. Lett. **123**, 065501 (2019).

[36] Q. B. Liu, Z. J. Wang, and H. H. Fu, Phys. Rev. B **103**, L161303 (2021).

[37] T. T. Zhang, H. Miao, Q. Wang, J. Q. Lin, Y. Cao, G. Fabbris, A. H. Said, X. Liu, H. C. Lei, Z. Fang *et al.*, Phys. Rev. Lett. **123**, 245302 (2019).

[38] B. Zheng, B. Xia, R. Wang, Z. Chen, J. Zhao, Y. Zhao, and H. Xu, Phys. Rev. B **101**, 100303(R) (2020).

[39] J. Y. You, X. L. Sheng, and G. Su, Phys. Rev. B **103**, 165143 (2021).

[40] D. S. Ma, K. J. Yu, X. P. Li, X. Y. Zhou, and R. Wang, arXiv:2210.14592.

[41] J. H. Wang, H. K. Yuan, M. Q. Kuang, T. Yang, Z. M. Yu, Z. Y. Zhang, and X. T. Wang, Phys. Rev. B **104**, L041107 (2021).

[42] M. Wang, Y. Wang, Z. Y. Yang, J. Fan, B. B. Zheng, R. Wang, and X. Z. Wu, Phys. Rev. B **105**, 174309 (2022).

[43] X. T. Wang, F. Zhou, T. Yang, M. Q. Kuang, Z. M. Yu, and G. Zhang, Phys. Rev. B **104**, L041104 (2021).

[44] G. Liu, Z. J. Chen, P. Wu, and H. Xu, Phys. Rev. B **106**, 214308 (2022).

[45] X. T. Wang, F. Zhou, Z. Y. Zhang, Z. M. Yu, and Y. G. Yao, Phys. Rev. B **106**, 214309 (2022).

[46] J. X. Li, J. X. Liu, S. A. Baronett, M. F. Liu, L. Wang, R. H. Li, Y. Chen, D. Z. Li, Q. Zhu, and X. Q. Chen, Nat. Commun. **12**, 1204 (2021).

[47] Y. J. Jin, Z. J. Chen, X. L. Xiao, and H. Xu, Phys. Rev. B **103**, 104101 (2021).

[48] Z. D. Jin, B. Y. Hu, Y. R. Liu, Y. M. Li, T. T. Zhang, K. Iida, K. Kamazawa, A. I. Kolesnikov, M. B. Stone, X. Y. Zhang *et al.*, Phys. Rev. B **106**, 224304 (2022).

[49] M. M. Zhong, Y. Liu, F. Zhou, M. Q. Kuang, T. Yang, X. T. Wang, and G. Zhang, Phys. Rev. B **104**, 085118 (2021).

[50] G. Liu, Z. Q. Huang, Z. J. Chen, Y. J. Jin, C. C. He, and H. Xu, Phys. Rev. B **106**, 054306 (2022).

[51] Y. Yang, F. Zhou, J. H. Wang, Y. Liu, Y. T. Cui, G. Q. Ding, and X. T. Wang, Appl. Phys. Lett. **122**, 232202 (2023).

[52] C. X. Cui, X. P. Li, D. S. Ma, Z. M. Yu, and Y. G. Yao, Phys. Rev. B **104**, 075115 (2021).

[53] Z. M. Yu, W. Wu, X. L. Sheng, Y. X. Zhao, and S. A. Yang, Phys. Rev. B **99**, 121106(R) (2019).

[54] Y. T. Oh, H. G. Min, and Y. Kim, Phys. Rev. B **99**, 201110(R) (2019).

[55] B. J. Wieder and C. L. Kane, Phys. Rev. B **94**, 155108 (2016).

[56] Z. Y. Zhang, Z. M. Yu, G. B. Liu, and Y. G. Yao, Comput. Phys. Commun. **270**, 108153 (2022).
[57] R. Yu, X. L. Qi, A. Bernevig, Z. Fang, and X. Dai, Phys. Rev. B **84**, 075119 (2011).
[58] M. I. Aroyo, J. M. Perez-Mato, D. Orobengoa, E. Tasci, G. de la Flor, and A. Kirov, Bulg. Chem. Commun. **43**, 183 (2011).
[59] See Supplemental Material at http://link.aps.org/supplemental/10.1103/PhysRevB.108.054305 for the computational method, the tight-binding model for space group 96, symmetry analysis, and more materials, which includes Refs. [61–69].
[60] J. Huster and W. Bronger, Z. Anorg. Allg. Chem. **630**, 642 (2004).
[61] W. Kohn and L. J. Sham, Phys. Rev. **140**, A1133 (1965).
[62] G. Kresse and J. Furthmüller, Phys. Rev. B **54**, 11169 (1996).
[63] J. P. Perdew, K. Burke, and M. Ernzerhof, Phys. Rev. Lett. **77**, 3865 (1996).
[64] J. P. Perdew, K. Burke, and M. Ernzerhof, Phys. Rev. Lett. **78**, 1396(E) (1997).
[65] G. Kresse and D. Joubert, Phys. Rev. B **59**, 1758 (1999).
[66] D. M. Ceperley and B. J. Alder, Phys. Rev. Lett. **45**, 566 (1980).
[67] A. Togo and I. Tanaka, Scr. Mater. **108**, 1 (2015).
[68] Q. S. Wu, S. N. Zhang, H. F. Song, M. Troyer, and A. A. Soluyanov, Comput. Phys. Commun. **224**, 405 (2018).
[69] M. P. L. Sancho, J. M. L. Sancho, and J. Rubio, J. Phys. F: Met. Phys. **14**, 1205 (1984).